Earlier onset of tumoral angiogenesis in matrix metalloproteinase-19 deficient mice

Maud Jost,[1] Alicia R. Folgueras,[2] Françoise Frérart,[1] Alberto M. Pendas,[2,3] Silvia Blacher,[1] Xavier Houard,[1] Sarah Berndt,[1] Carine Munaut,[1] Didier Cataldo,[1] Jesus Alvarez,[2] Laurence Melen-Lamalle,[1] Jean-Michel Foidart,[1,4] Carlos López-Otín,[2] and Agnès Noël[1]*

[1]Laboratory of Tumor and Developmental Biology, Center for Experimental Cancer Research (CECR), Center for Biomedical Integrative Genoproteomics (CBIG), University of Liège, Tour de Pathologie (B23), B-4000 Sart-Tilman, Belgium, [2]Departamento de Bioquímica y Biología Molecular, Facultad de Medicina, Instituto Universitario de Oncología, Universidad de Oviedo, 33006-Oviedo, Spain, [3]Centro Investigacion Cancer, Salamanca, Spain, [4]Department of Gynecology, CHU, 4000 Liège.

Running title: MMP-19 and tumoral angiogenesis

Corresponding author:

A. NOEL

Laboratory of Tumor and Developmental Biology

University of Liège, Tour de Pathologie (B23)

Sart-Tilman, B-4000 Liège

Tel : +32-4-366.25.69 ; Fax: +32-4-366.29.36

E-mail: agnes.noel@ulg.ac.be

Abstract

Among matrix metalloproteinases (MMPs), MMP-19 displays unique structural features and tissue distribution. In contrast to most MMPs, MMP-19 is expressed in normal human epidermis and downregulated during malignant transformation and dedifferentiation. The contribution of MMP-19 during tumor angiogenesis is presently unknown. In an attempt to give new insights into MMP-19 *in vivo* functions, angiogenic response of mutant mice lacking *Mmp-19* was analysed after transplantation of murine malignant PDVA keratinocytes and after injection of matrigel supplemented with b-FGF. *In situ* hybridization and immunohistochemical analysis revealed that MMP-19 is produced by host mesenchymal cells, but not by endothelial capillary cells or CD11b-positive inflammatory cells. Based on a new computer-assisted method of quantification, we provide evidence that host *Mmp-19* deficiency was associated with an increased early angiogenic response. In addition, increased tumor invasion was observed in *Mmp-19-/-* mice. We conclude that, in contrast to most MMPs which promote tumor progression, Mmp-19 is a negative regulator of early steps of tumor angiogenesis and invasion. These data highlight the requirement to understand the individual functions of each MMP in order to improve anti-cancer strategies.

Introduction

Matrix metalloproteinases (MMPs) are a family of structurally related zinc-dependent neutral endopeptidases that play major roles in tissue remodeling occurring in a variety of physiological processes such as embryonic development, angiogenesis and wound healing (1, 2). They are main effectors of pathological extracellular matrix destruction in many diseases such as arthritis, atherosclerosis, age-related macular degeneration, tumor invasion and metastasis (3-7). MMPs contribute to the fine tuning of diverse biological processes through limited proteolysis of specific targets including not only matrix components, but also growth factors, chemokines/cytokines and cell surface receptors (8-11). More than 20 different human MMPs have been identified (12) and classified into different subfamilies according to their primary structure, domain organization, cellular localization and substrate specificity (11, 13, 14). Produced as latent forms, they are either secreted in the extracellular medium or associated to the cell membrane (Membrane-type MMPs or MT-MMPs) (7, 11, 14).

Among MMPs, MMP-19 displays unique structural features and tissue distribution. Human MMP-19 cDNA was initially cloned from liver and mammary gland and was also identified as an autoantigen in inflamed rheumatoid synovium (15, 16). MMP-19 presents the typical domain organization of soluble MMPs, including a signal sequence, a propeptide maintaining enzyme latency, a catalytic domain with the typical zinc binding motif, a linker region, and a C-terminal fragment with sequence similarity to hemopexin (15). However, MMP-19 displays several structural features distinctive of the diverse MMP subfamilies including (i) an unique insertion of glutamic acid residues within the linker region, (ii) an unusual latency motif in propeptide domain, (iii) an additional cysteine residue in catalytic region, (iv) a C-terminal extension lacking

sequence similarity to equivalent regions in other human MMPs (15, 17, 18). The catalytic domain of MMP-19 is capable of degrading components of basement membrane (laminin, type IV collagen, nidogen), connective tissue (fibronectin, type I gelatine) and cartilage (cartilage oligomeric matrix protein and aggrecan), but does not degrade triple-helical type I collagen (19, 20). In contrast to most other MMPs, MMP-19 is expressed in human mammary or skin epithelial cells under normal quiescent conditions and down regulated in invasive carcinomas (21-23).

Evidence for MMP-19 involvement in tissue remodeling events such as those occurring during adipogenesis and tumor progression have been provided by the recent generation of *Mmp-19*-deficient mice (24). Although lack of *Mmp-19* did not affect mice viability, fertility and development, it led to a diet-induced obesity and a decreased susceptibility to skin tumors induced by chemical carcinogens. A role of MMP-19 during angiogenesis is suggested by its expression in endothelial cells of synovial capillaries following injury and inflammation (3, 25). However, the *ex vivo* sprouting of endothelial cells from aortic rings was not affected by *Mmp-19* deficiency (24). Therefore, the contribution of MMP-19 during angiogenic processes remains controversial. In order to give new insights into Mmp-19 functions *in vivo*, the angiogenic response of mutant mice lacking *Mmp-19* was analysed after transplantation of malignant murine PDVA keratinocytes and after injection of matrigel supplemented with b-FGF. In contrast to other single or double MMP-deficient mice studied until now, *Mmp-19*-deficient mice exhibited an early onset of angiogenesis and tumor invasion.

Materials and Methods

Mmp-19–null mice. Mice genetically deficient in Mmp-19 (*Mmp-19-/-*) were generated by replacing a portion of 1kb of the promoter and exons 1 and 2 of the gene with a phosphoglycerate kinase-neomycin fusion gene and by homologous recombination (24). Homozygous *Mmp-19* (*Mmp-19-/-*) mice and their corresponding WT (*Mmp-19+/+*) were littermates deriving from interbreeding of heterozygotes with a mixed background of C57Bl6/129Ola. When applying the transplantation chamber assay to mice with different genetic background, we previously demonstrated that the extent of tumor invasion and vascularization was similar in all WT mice, independently to the number of backcrosses in C57Bl6 mice (26). Mice experimentation was done in accordance to guidelines of the University of Liège regarding the care and use of laboratory animals.

Transplantation assay in mice. PDVA cells were generated by *in vitro* carcinogen treatment (DMA) of cultured keratinocytes issued from B10LP mice (27). PDVA cells were grown in modified Eagle's minimal essential medium containing a 4-fold concentration of amino acids and vitamins (Gibco Laboratories, Grant Island, NY), 10% fetal calf serum (Gibco) and antibiotics in a humidified incubator at 37 °C, 5% CO2. Cells (2 x 10^5) were seeded on a collagen gel (4 mg/mL of type I collagen isolated from rat tail tendons) inserted in Teflon rings (Renner GmbH, Dannstadt, Germany). After 24h of culture, cell-coated collagen gels were covered with a silicone transplantation chamber (Renner GmbH) and implanted in toto onto dorsal muscle fascia of 6-8 weeks old mice according to the procedure previously described (28, 29). At different time points, tumor transplants were resected, embedded in Tissue Tek (Miles Laboratories Inc., Naperville, IL) and frozen in liquid nitrogen for cryostat sectioning. Two hours

prior to sacrifice, mice were intraperitonally injected with 200 µl of BrdU/BrdC (65 µM, Acros Organics, Geel, Belgium). Each experimental group contained at least 6 animals. Tumor angiogenesis and invasion in *Mmp-19-/-* and WT mice were evaluated in three independent sets of experiment.

Histological analysis. Cryostat sections were fixed in acetone at –20°C and in 80% methanol at 4°C. For immunofluorescence labeling, the following antibodies were used: anti-type IV collagen Ab (rabbit polyclonal Ab; diluted 1/100), anti-keratin Ab (polyclonal guinea pig Ab; diluted 1/20, Sigma-Aldrich, St Louis, MO), anti-BrdU-FITC (monoclonal mouse, diluted 1/3.5, Becton Dickinson, San Diego, CA), anti-hinge region of MMP-19 (rabbit anti-human, diluted 1/20, Sigma-Aldrich; rabbit anti-human, diluted 1/500, Abcam, Cambridge, MA), anti- MMP-19 prodomain (rabbit anti-human, diluted 1/500, Abcam), anti-CD11b/TRITC (rat anti-mouse, diluted 1/50, Pharmingen, San Diego, CA), anti α-smooth muscle actin/FITC (α-SMA) (monoclonal mouse antibody, diluted 1/200, Sigma-Aldrich). When double immunofluorescence-labelings were performed, after an incubation for 1 h with primary antibodies, sections were washed with phosphate buffered saline (PBS) and then incubated for 30 min with fluorescein-isothiocyanate (FITC)- or tetramethyl-rhodamine isothiocyanate (TRITC)-conjugated appropriate secondary antibodies: swine anti-rabbit (diluted 1/40, Dako, Glostrup, Denmark,), mouse anti-guinea pig (diluted 1/40, Sigma-Aldrich) or goat anti-rat (diluted 1/100, Molecular Probes, Carlsbad, CA). After 3 washes in PBS, coverslips were mounted with Aqua Polymount (Polysciences, Warrington, FL) and specific labeling was observed using an inverted microscope equipped with epifluorescence optics. Sections were counterstained in blue with bisbenzimide. At all times after grafting, collagen type IV labelings were codistributed with endothelial cells recognized by the anti-mouse PECAM immunostaining (data not shown).

Apoptosis was studied by terminal deoxynucleotidyl transferase (TDT)-mediated deoxyuridine triphosphate (dUTP) nick-end labeling (TUNEL). Cryostat sections fixed in 4% paraformaldehyde for 20 min and in methanol for 5 min were stained for apoptosis following manufacturer's instructions (Roche Diagnostics, Mannheim, Germany).

For quantitative measurement of proliferating cells, automatic computer-assisted image analysis was performed on images obtained after bisbenzimide staining and immunolabeling of BrdU positive cells. The ratio between the surface of bisbenzimide staining and the surface of specific immunostaining was measured by using a software Aphelion 3.2 from Adsis.

In situ hybridization: Either sense or antisense ^{35}S-uridine triphosphate-labeled RNA probes were synthesized from linearized cDNA fragment (1600 bp) of mouse *Mmp-19* gene cloned into EcoRV site of pcDNA3. Cryostat sections were hybridized with ^{35}S-labeled Mmp-19 riboprobes and then exposed to photographic emulsion at 4°C for 6 days. Sections were developed, fixed, cleared and counterstained with 0.02% Toluidine Blue. Bright field and dark field images were captured with a SPOT digital camera.

Scoring of tumor invasion and vascularization. For semi-quantitative analysis of tumor vascularization, the following scoring was used: +: vessels below the collagen gel or infiltrating the collagen gel without reaching the malignant epithelial layer; ++: blood vessels in close apposition to the epithelial layer, and +++: blood vessels intermingled with invasive epithelial tumor sprouts (29).

Morphometric measurements of tumor cell invasion (average distance of

invasion) and tumor vascularization (endothelial cell migration) were performed by using a computer-assisted image analysis system (Olympus Micro Image version 3.0 for Windows 95/NT, Olympus Optical CO. Europe GmBH) (30). Angiogenesis was quantified by measuring the distance ("d") separating tumor cells from the front of migrating blood vessels. Therefore, the distance "d" is inversely related to the degree of endothelial cell migration. At least five measurements of distance ("d") were performed in the central part of each tumor and the mean values are reported.

Quantitative measurement of tumor invasion and angiogenesis by computer-assisted image processing. For quantitative measurements, automatic computer-assisted image analysis was performed on images obtained after double immunostainings of keratinocytes (in green) and vessels (in red). The software Aphelion 3.2 from Adsis was used on a PC. Images were first digitized in 760 x 570 pixels with 256 grey levels. Tumor and vessels images were processed separately. For tumor images, histogram equalization was first performed in order to optimize the contrast. Then, tumor images were binarized/segmented automatically using the entropy of the histogram of the grey level intensities (31). For vessel images, vessels were binarized/segmented using an automatic threshold transformation that maximizes the global average contrast of edges (32). The upper boundary of the tumor was then automatically detected using a hit or miss transformation with an appropriate neighborhood configuration. A grid was constructed with the successive dilations (n=1, 2, 3….) of this upper boundary, with a vertical line as structuring element. Tumor and vessel densities were determined on each interval of the grid, and the results drawn in function of the distance to the upper limit of the tumor. The largest distance of tumor invasion gives the thickness of the tumor. Quantification was performed on each mouse in all independent assays. To compare the different distributions, the analysis of

variance was performed and results were considered significantly different when the p-value was less than 0.05.

Matrigel plug assay. A total of 0.5 ml of Matrigel (10mg/ml) mixed with 250 ng of basic Fibroblast Growth Factor (bFGF) (R&D Systems, Mineapolis, MN) and 20U of heparin (Leo Pharma, Ballerup, Denmark) (33) was subcutaneously injected in the abdominal midline region of 8 week-old *Mmp-19* null and wild-type mice. After 7 days, animals were euthanized and Matrigel implants were harvested, frozen on dry ice and lyophilized overnight. Dry plugs were weight and suspended in 0.4ml of 0.1% saponin (Calbiochem, La Jolla, CA) for 1 h at 4°C, disrupted by vigorous pipetting and centrifuged at 15,000g for 15 min, at 4°C to remove particulates. Concentration of haemoglobin in the supernatant was determined after dilution in Drapkin's solution by measuring the absorbance at 560 nm (Drabkin reagent kit 525, Sigma). A standard curve was performed by using purified haemoglobin (Sigma). The angiogenic index corresponds to μg of haemoglobin per mg of Matrigel.

Statistical analysis. All experimental data are reported as mean ± SEM, and statistical analysis was performed by χ^2 test or Mann-Whitney test. $P < 0.05$ was considered as significant.

Results

Lack of *Mmp-19* increased the onset of skin tumor vascularization. Malignant PDVA keratinocytes cultured on a collagen gel were implanted onto the dorsal muscle fascia of *Mmp-19-/-* and *Mmp-19+/+* mice. In order to compare evolution of tumor invasion and vascularization in these genotypes, transplants were resected after 14 and 21 days and angiogenesis was visualized after staining for collagen type IV to delineate capillary basement membranes (Fig. 1). Tumor grafting led to a remodeling of collagen matrix and a progressive infiltration by host-derived cells including endothelial cells and inflammatory cells. Tumor vascularization was semi-quantitatively scored according to the progressive migration of blood vessels towards tumor cells (Fig. 1). At day 14, in *Mmp-19+/+* mice, blood vessels remained below the collagen gel or started to infiltrate it and all samples were scored + (Fig. 1*A*). Tumor vascularization in *Mmp-19-/-* mice was increased since 63% and 37% of transplants were scored + and ++, respectively (Fig. 1*B*) ($P<0.05$, χ^2 test). At that time, in both genotypes, tumor layer appeared as an irregular stratified epithelium on top of the collagen gel (Fig. 1*A*).

Vascularization of tumor transplants at day 14 was first quantified by measuring the distance ("d") separating the bottom of tumor layer from the front of migrating blood vessels (Fig. 1*D*). This parameter is inversely related to the degree of endothelial cell migration. Compared to *Mmp-19+/+* mice, vessels migrated over a higher distance in *Mmp-19*-deficient mice (Fig. 1*D*). Indeed, the distance separating endothelial cells to malignant keratinocytes was 2.5 fold reduced in *Mmp-19* null mice than in their corresponding wild-type littermates ($P=0.0062$, Mann-Whitney test)(Fig. 1*D*).

The observed increased blood vessel migration in *Mmp-19*-null mice prompted us to set up a more objective quantitative method to investigate the spatial distribution of

blood vessels in the remodeled matrix. With this aim, an original method based on computer-assisted image analysis was developed (Fig. 2). The density of vessels picked already at a distance of around 0.25 mm from the upper boundary of tumor layer in *Mmp-19*-/- mice (Fig. 2*B*). In sharp contrast, the maximal density of endothelial cells was observed at a distance of around 0.75 mm in *Mmp-19*+/+ mice. A computer-assisted method of image analysis was also set up to quantify tumor cell invasion (Fig. 2*A*). At day 14 time point, no invasion was observed (Fig. 2*C*). This was expected since in the transplantation chamber assay, infiltration of vessels through the collagen gel towards tumor cells always precedes recognizable tumor cell invasion (34). Therefore, at early time point, *Mmp-19*-deficient mice exhibited an acceleration of blood vessel infiltration in the remodeled matrix.

Lack of *Mmp-19* increased tumor invasion

At day 21, once blood vessels have reached tumor cell layers, malignant keratinocytes formed tumor sprouts that invaded downwards the remodeled host tissue and were intermingled with closely apposed new vessels (Fig. 1*A*). Such vascularization pattern scored +++ was observed in about 60% (10/17) of *Mmp-19-/-* mice and only 22% (4/18) of *Mmp-19*+/+ mice ($P = 0.027$, χ^2 test) (Fig. 1*C*).

At this time point, the distance ("d") separating tumor layer from the front of recruited blood vessels (Fig. 1) can not be measured since in more than 70% of tumor transplants, vessels have reached the tumor layer (tumors scored ++ or +++). Therefore, for quantitative assessment, our original method of image analysis (Fig. 2) was applied to determine the malignant keratinocyte density as a function of the distance to the top of tumor transplant (Fig. 2*D*). In wild-type mice, keratinocyte density decreased abruptly with the distance to the top of tumor layer (Fig. 2*D*). Only few keratinocytes

were observed at a distance higher than 0.5 mm from the top of tumor layer. In sharp contrast, in *Mmp-19* null mice, tumor cell density decreased more slowly and numerous malignant keratinocytes migrated over a distance of 0.5 mm. The maximal distance of keratinocyte migration was 1.2 mm and 1.8 mm in *Mmp-19*+/+ and *Mmp-19*-/- mice, respectively (Fig. 2*D*). Therefore, a significant increase of tumor invasion was observed in the absence of host *Mmp-19*.

This tumor promoting effect observed in absence of Mmp-19 was not related to a modification of tumor cell proliferation rate as assessed by BrdU incorporation. Indeed, quantitative assessment performed by computer-assisted image analysis revealed that the percentage of proliferating cells was similar in both genotypes, 14 and 21 days after tumor transplantation (Fig. 3). Furthermore, TUNEL stainings for apoptotic cells indicated that the extent of apoptosis was identical and always low in cancer cell layers as well as in stromal strands of transplants resected from WT mice and *Mmp-19-/-* mice (data not shown).

Mmp-19 is produced by host stromal cells

As a first step in determining the cellular source of Mmp-19, *in situ* hybridization was performed on tumors transplanted into *Mmp-19* proficient and deficient mice. Hybridization signals for Mmp-19 mRNAs were found in the stroma of WT mice (Fig. 4*A*), but not in that of KO mice (Fig. 4*C*). No positive signal was detected after treatment with sense riboprobe used as negative controls (Fig. 4*B*). Immunohistochemical staining of tumor transplants confirmed the stromal production of Mmp-19 (Fig. 5*A*). This protease was produced by mesenchymal cells (Fig. 5*A*), but not by inflammatory cells positive for CD11b staining (Fig. 5*C*). Interestingly, Mmp-19 was not associated with capillaries newly formed in the remodelled collagen matrix

(data not shown). In contrast, Mmp-19 staining was detected in large vascular structures present deeply in the host tissue, below tumor transplants (Fig. 5*B*). These vessels were positive for α-smooth muscle actin and correspond to quiescent mature vessels.

Lack of *Mmp-19* increased angiogenesis in Matrigel plug assay

To further investigate the impact of Mmp-19 deficiency on angiogenesis *in vivo* and to determine whether the angiogenic response was dependent upon the matrix encountered by endothelial cells during their migration, the Matrigel plug assay was applied to mutant mice. Matrigel supplemented with bFGF was sub-cutaneously injected into the abdomen of wild type and mutant mice (n = 8) and harvested after 7 days. Quantitative analysis of angiogenesis was performed by measuring haemoglobin content in implants giving quantitative information on functional vessels. In accordance to results obtained in transplantation chamber assay, the angiogenic response in *Mmp-19* deficient mice was 6-fold increased as compared to that detected in wild type mice (Fig. 6) ($P < 0.05$) and was therefore independent on the type of matrix used (type I collagen *versus* a reconstituted basement membrane).

Discussion

The analysis of cancer susceptibility in individual *Mmp*-null mice is of growing interest after the failure of synthetic MMP inhibitors in clinical trials and the finding of multiple and even opposite roles of MMPs in tumor progression. We describe here that in contrast to most MMP deficiencies described up to now in mice, the angiogenic response was accelerated and tumor invasion was increased in *Mmp-19*-deficient mice. This was evidenced by (i) an accelerated vascularization and a higher degree of tumor invasion after malignant keratinocyte transplantation and (ii) an increased vascularization in bFGF treated matrigel implants in *Mmp-19-/-* mice.

The time course of malignant growth begins with an early onset of stromal activation and infiltration of inflammatory cells and endothelial cells. These key events can be mimicked in the transplantation system used here which is a highly sensitive tool to inspect kinetics of early steps of host stromal response to tumor signals (34, 35). By applying this system to *Mmp-19-/-* mice, it appears that the angiogenic response was affected by lack of host Mmp-19. Surprisingly, endothelial cell recruitment was significantly increased 14 days after transplantation, leading to an acceleration of tumor vascularization. Consequently, tumor invasion was increased in *Mmp-19*-deficient mice, 21 days after tumor transplantation. These findings indicate that Mmp-19 is a negative regulator of early steps of cancer angiogenesis and invasion.

By *in situ* hybridization and immunohistochemical analysis, we demonstrate that mesenchymal cells produce Mmp-19, while CD11b-positive inflammatory cells and malignant keratinocytes do not express it. Accordingly, MMP-19 mRNA expression and pro-MMP-19 production by human fibroblasts have been detected *in vivo* in dermal wounds and in cultures of fibroblasts (36). In our model, Mmp-19 is not produced by

sprouting endothelial cells of neo-formed capillaries. This observation fits with our previous observation that Mmp-19 is not required for *ex vivo* endothelial cell migration in a collagen gel in the aortic ring assay (24). According to the report of Kolb C et al. (25), Mmp-19 is associated with αSMA positive large vessels deeply embedded in the host tissue.

Taking into account its *in vitro* substrates (laminin-1, laminin-5, type IV collagen, fibronectin, tenascin-C or nidogen), MMP-19 might play a key role in matrix degradation and tissue remodeling (19, 20, 37). A recent *in vitro* study suggests that through its capacity to cleave nidogen, Mmp-19 could control formation of capillary structures on matrigel by cultured endothelial cells (38). However, the *ex vivo* endothelial cell sprouting from mouse aortic rings in a three dimensional matrix was not affected by *Mmp-19* deficiency (24). Therefore, the accelerated angiogenic response observed *in vivo* in the transplantation system could not be ascribed to a modified ability of endothelial cells to migrate or differentiate into capillary-like structures in a pure collagen matrix, in the absence of Mmp-19. Interestingly, the accelerated recruitment of endothelial cells *in vivo* was observed both in transplantation system using type I collagen and in Matrigel plug assay suggesting that this effect of Mmp-19 on angiogenesis was not dependent upon the matrix used.

The identification of novel non matrix substrates for MMPs has extended MMP functions beyond their classical role in ECM disruption (4, 11). The recent finding that Mmp19 cleaves *in vitro* IGFBP-3 (39) suggests that it could control the activity of insulin-like growth factors and thereby regulate cancer cell growth. However, in our system, tumor cell proliferation was not affected by Mmp-19 deficiency. Similarly, tumor cell apoptosis was not modulated by the absence of host Mmp-19. It is worth

noting that proteolytic processing of some bioactive molecules such as growth factors and/or cytokines/chemokines could also indirectly contribute to micro-environment modifications promoting or inhibiting endothelial cell recruitment during angiogenesis onset. The assumption that MMPs are in general pro-angiogenic has been challenged by the finding that some of them could suppress neovascularization by generating angiogenic inhibitors (40). In this context, Mmp-19 could exert its anti-angiogenic effect through inactivation of angiogenic/chemotactic factors or production/maturation of angiogenic inhibitors. In addition, Mmp-19 production in large quiescent host vessels present below tumor transplants, but not in growing capillaries suggests a yet unknown functional role of this protease in maintenance of blood vessel stability. Its absence could destabilize endothelial cell-mural cell interactions, thereby initiating active sprouting events and endothelial cell migration. This hypothesis could explain the transient effect of Mmp-19 deficiency at angiogenesis onset.

The present results do not negate the possibility that Mmp-19 might have dual functions during cancer progression. In a model of methylcholanthrene-induced chemical carcinogenesis, we previously showed that *Mmp-19*-/- mice develop less fibrosarcomas and with a longer latency period than wild-type littermates (24). These apparently paradoxical results may reflect different roles of Mmp-19 in the evolution of various cancer types (carcinoma *versus* fibrosarcoma), as well as throughout different steps of cancer progression. The down-regulation and disappearance of MMP-19 production observed during neoplastic progression in breast and skin carcinomas (21-23) are consistent with our data demonstrating a control of early steps of skin carcinoma evolution by Mmp-19. Altogether these data based on clinical and experimental studies suggest that MMP-19 negatively regulates early stages of tumor cell invasion, but cancer cells could become less sensitive to MMP-19 activity once tumor develops.

Temporal differences in effect of proteases on tumor growth and conversion to aggressive tumors have also been reported for Mmp-9 (41) and Mmp-11 (42).

By applying the same transplantation chamber assay into different single or double *Mmp*-deficient mice (43), we previously reported that tumor invasion and angiogenesis were both impaired by the combined deficiency in *Mmp-2* and *Mmp-9* demonstrating that concomitant production of gelatinases is required for tumor invasion and vascularization. Therefore, although Mmp-2 and Mmp-9 are viewed as positive regulators of tumor angiogenesis (4, 44-46), Mmp-19 could function in an opposite manner, slowing-down the angiogenic process. These unexpected data are in accordance with the emerging anti-tumor properties of some MMPs. In this context, skin tumor susceptibility was increased in mice deficient for Mmp-8 (47) or Mmp-3 (48). Furthermore, our results support the view that MMPs act as sophisticated modulators rather than simple inducers or suppressors and highlight the functional complexity of MMP family during cancer progression. Some MMPs appear to have dual role in cancer progression by promoting angiogenesis and generating angiogenesis inhibitors (6). For instance, although MMP-7 and MMP-9 are both able to generate angiostatin (40), MMP-7 facilitates tumor progression in mouse models (49) and MMP-9 promotes tumor angiogenesis (43-46). Increased expression of some MMPs may both confer increased tumor cell invasiveness and paradoxically, lead to production of molecules that limit tumor growth. Altogether, these data point out the need to determine both spatial and temporal significance of individual MMP during cancer progression in order to design more rational MMP inhibitors.

Acknowledgments

We thank I. Dasoul, P. Gavitelli, F. Olivier and G. Roland for their excellent technical assistance. This work was supported by grants from the Communauté Française de Belgique (Actions de Recherches Concertées), the European Union (FP5 and FP6), the Fonds National de la Recherche Scientifique (FNRS, Belgium), the Fédération Belge Contre le Cancer, the Centre Anticancéreux près l'Université de Liège, the FB Assurances, the Fondation Léon Frédéricq (University of Liège), the D.G.T.R.E. from the "Région Wallonne", the Interuniversity Attraction Poles Programme- Belgian Science Policy (Brussels, Belgium), the Comision Interministerial de Ciencia y Tecnologia (to C. L.-O). M.J. and S.B are recipients of a grant from FNRS-Télévie. D.C. is a scientific research worker from the FNRS (Belgium).

References

1. Nagase H, Woessner JF. Matrix metalloproteinases. J Biol Chem 1999;274:21491-4.

2. Vu TH, Werb Z. Matrix metalloproteinases: effectors of development and normal physiology. Genes Dev 2000;14:2123-33.

3. Konttinen YT, Ainola M, Valleala H et al. Analysis of 16 different matrix metalloproteinases (MMP-1 to MMP-20) in the synovial membrane: different profiles in trauma and rheumatoid arthritis. An Rheum Dis 1999;58:691-7.

4. Folgueras AR, Pendas AM, Sanchez LM, Lopez-Otin C. Matrix metalloproteinases in cancer: from new functions to improved inhibition strategies. Int J Dev Biol 2004;48:411-24.

5. Noel A, Maillard C, Rocks N et al. Membrane associated proteases and their inhibitors in tumour angiogenesis. J Clin Pathol 2004;57:577-84.

6. Handsley MM, Edwards DR. Metalloproteinases and their inhibitors in tumor angiogenesis. Int J Canc 2005;115:849-60.

7. Sounni NE, Noel A. Membrane type-matrix metalloproteinases and tumor progression. Biochimie 2005;87:329-42.

8. Sternlicht MD, Werb Z. How matrix metalloproteinases regulate cell behavior. Annu Rev Cell Dev Biol 2001;17:463-516.

9. McQuibban GA, Gong JH, Tam EM, McCulloch CAG, Clark-Lewis I, Overall CM. Inflammation dampened by gelatinase A cleavage of monocyte chemoattractant protein-3. Science 2000;289:1202-6.

10. McQuibban GA, Butler GS, Gong JH et al. Matrix metalloproteinase activity inactivates the CXC chemokine stromal cell-derived factor-1. J Biol Chem 2001;276:43503-8.

11. Egeblad M, Werb Z. New functions for the matrix metalloproteinases in cancer progression. Nat Rev Cancer 2002;2:161-74.

12. Puente XS, Lopez-Otin C. A genomic analysis of rat proteases and protease inhibitors. Genome Res 2004;14:609-22.

13. Lopez-Otin C, Overall CM. Protease degradomics: A new challenge for proteomics. Nat Rev Mol Cell Biol 2002;3:509-19.

14. Zucker S, Pei DQ, Cao J, Lopez-Otin C. Membrane type-matrix metalloproteinases (MT-MMP). Cell Surface Proteases 2003;54:1-74.

15. Pendas AM, Knauper V, Puente XS et al. Identification and characterization of a novel human matrix metalloproteinase with unique structural characteristics, chromosomal location, and tissue distribution. J Biol Chem 1997;272:4281-6.

16. Sedlacek R, Mauch S, Kolb B et al. Matrix metalloproteinase MMP-19 (RASI 1) is expressed on the surface of activated peripheral blood mononuclear cells and is detected as an autoantigen in rheumatoid arthritis. Immunobiology 1998;198:408-23.

17. Yang MZ, Kurkinen M. Cloning and characterization of a novel matrix metalloproteinase (MMP), CMMP, from chicken embryo fibroblasts - CMMP, Xenopus XMMP, and human MMP19 have a conserved unique cysteine in the catalytic domain. J Biol Chem 1998;273:17893-900.

18. Mueller MS, Mauch S, Sedlacek R. Structure of the human MMP-19 gene. Gene 2000;252:27-37.

19. Stracke JO, Fosang AJ, Last K et al. Matrix metalloproteinases 19 and 20 cleave aggrecan and cartilage oligomeric matrix protein (COMP). Febs Letters 2000;478:52-6.

20. Stracke JO, Hutton M, Stewart M et al. Biochemical characterization of the catalytic domain of human matrix metalloproteinase 19 - Evidence for a role as a potent basement membrane degrading enzyme. J Biol Chem 2000;275:14809-16.

21. Djonov V, Hogger K, Sedlacek R, Laissue J, Draeger A. MMP-19: cellular localization of a novel metalloproteinase within normal breast tissue and mammary gland tumours. J Pathol 2001;195:147-55.

22. Impola U, Toriseva M, Suomela S et al. Matrix metalloproteinase-19 is expressed by proliferating epithelium but disappears with neoplastic dedifferentiation. Int J Canc 2003;103:709-16.

23. Impola U, Jeskanen L, Ravanti L et al. Expression of matrix metalloproteinase (MMP)-7 and MMP-13 and loss of MMP-19 and p16 are associated with malignant progression in chronic wounds. Br J Dermatol 2005;152:720-6.

24. Pendas AM, Folgueras AR, Llano E et al. Diet-induced obesity and reduced skin cancer susceptibility in matrix metalloproteinase 19-deficient mice. Mol Cell Biol 2004;24:5304-13.

25. Kolb C, Mauch S, Krawinkel U, Sedlacek R. Matrix metalloproteinase-19 in capillary endothelial cells: Expression in acutely, but not in chronically, inflamed synovium. Exp Cell Res 1999;250:122-30.

26. Bajou K, Masson V, Gerard RD et al. The plasminogen activator inhibitor PAI-1 controls in vivo tumor vascularization by interaction with proteases, not vitronectin: Implications for antiangiogenic strategies. J Cell Biol 2001;152:777-84.

27. Fusenig, N. E. Growth and differentiation characteristics of transformed keratinocytes from mouse and human skin in vitro and in vivo. Breitkreutz, D., Dzarlieva, R. T., Boukamp, P., Bohnert A., and Tilgen, W. J Invest Dermatol 1983;81, 168s-75s.

28. Bajou K, Noel A, Gerard RD et al. Absence of host plasminogen activator inhibitor 1 prevents cancer invasion and vascularization. Nat Med 1998;4:923-8.

29. Bajou K, Masson V, Gerard RD et al. The plasminogen activator inhibitor PAI-1 controls in vivo tumor vascularization by interaction with proteases, not vitronectin: Implications for antiangiogenic strategies. J Cell Biol 2001;152:777-84.

30. Bajou K, Maillard C, Jost M et al. Host-derived plasminogen activator inhibitor-1 (PAI-1) concentration is critical for in vivo tumoral angiogenesis and growth. Oncogene 2004;23:6986-90.

31. Kapur, J. N., Sahoo, P. K, and Wong, A. K. C. A New Method for Gray-Level Picture Thresholding Using the Entropy of the Histogram. Computer Vision, Graphics, and Image Processing 29. 1985.

32. Kohler, R. A Segmentation System Based on Thresholding. Computer Graphics and Image Processing 1985;15, 319-38.

33. Passaniti A, Taylor RM, Pili R et al. Methods in Laboratory Investigation - A Simple, Quantitative Method for Assessing Angiogenesis and Antiangiogenic Agents Using Reconstituted Basement-Membrane, Heparin, and Fibroblast Growth-Factor. Laboratory Investigation 1992;67:519-28.

34. Mueller MM, Fusenig NE. Tumor-stroma interactions directing phenotype and progression of epithelial skin tumor cells. Differentiation 2002;70:486-97.

35. Mueller MM, Fusenig NE. Friends or foes - Bipolar effects of the tumour stroma in cancer. Nat Rev Cancer 2004;4:839-49.

36. Hieta N, Impola U, Lopez-Otin C, Saarialho-Kere U, Kahari VM. Matrix metalloproteinase-19 expression in dermal wounds and by fibroblasts in culture. J Invest Dermatol 2003;121:997-1004.

37. Sadowski T, Dietrich S, Koschinsky F et al. Matrix metalloproteinase 19 processes the laminin 5 gamma 2 chain and induces epithelial cell migration. CMLS 2005;62:870-80.

38. Titz B, Dietrich S, Sadowski T, Beck C, Petersen A, Sedlacek R. Activity of MMP-19 inhibits capillary-like formation due to processing of nidogen-1. CMLS 2004;61:1826-33.

39. Sadowski T, Dietrich S, Koschinsky F, Sedlacek R. Matrix metalloproteinase 19 regulates insulin-like growth factor-mediated proliferation, migration, and adhesion in human keratinocytes through proteolysis of insulin-like growth factor binding protein-3. Mol Biol Cell 2003;14:4569-80.

40. Pozzi A, Moberg PE, Miles LA, Wagner S, Soloway P, Gardner HA. Elevated matrix metalloprotease and angiostatin levels in integrin alpha 1 knockout mice cause reduced tumor vascularization. Proc Natl Acad Sci U S A 2000;97:2202-7.

41. Coussens LM, Tinkle CL, Hanahan D, Werb Z. MMP-9 supplied by bone marrow-derived cells contributes to skin carcinogenesis. Cell 2000;103:481-90.

42. Andarawewa KL, Boulay A, Masson W et al. Dual stromelysin-3 function during natural mouse mammary tumor virus-ras tumor progression. Cancer Res 2003;63:5844-9.

43. Masson V, de la Ballina LR, Munaut C et al. Contribution of host MMP-2 and MMP-9 to

promote tumor vascularization and invasion of malignant keratinocytes. FASEB J 2005;19:234-6.

44. Bergers G, Brekken R, McMahon G et al. Matrix metalloproteinase-9 triggers the angiogenic switch during carcinogenesis. Nat Cell Biol 2000;2:737-44.

45. Chantrain CF, Shimada H, Jodele S et al. Stromal matrix metalloproteinase-9 regulates the vascular architecture in neuroblastoma by promoting pericyte recruitment. Cancer Res 2004;64:1675-86.

46. Coussens LM, Tinkle CL, Hanahan D, Werb Z. MMP-9 supplied by bone marrow-derived cells contributes to skin carcinogenesis. Cell 2000;103:481-90.

47. Balbin M, Fueyo A, Tester AM et al. Loss of collagenase-2 confers increased skin tumor susceptibility to male mice. Nat Genet 2003;35:252-7.

48. Andarawewa KL, Boulay A, Masson W et al. Dual stromelysin-3 function during natural mouse mammary tumor virus-ras tumor progression. Cancer Res 2003;63:5844-9.

49. Rudolph-Owen LA, Chan R, Muller WJ, Matrisian LM. The matrix metalloproteinase matrilysin influences early-stage mammary tumorigenesis. Cancer Res 1998;58:5500-6.

Legends of figures:

Figure 1. *A*: Histological analysis of tumor transplants: Immunofluorescence labeling of malignant keratinocytes and vessels in tumors transplanted into *Mmp-19*+/+ or *Mmp-19*-/- mice observed after 14 (D14) or 21 (D21) days. Malignant cells (anti-keratin Ab in green) and vessels (anti-collagen type IV Ab in red) are visualized. The dotted line delineates the front of endothelial cell migration. Scores and morphometric parameter (d) used to quantify tumor invasion and angiogenesis are indicated (original magnification x200). *B-C*: Semi-quantitative evaluation of tumor vascularization in *Mmp-19*+/+ (black) or *Mmp-19*-/- mice (white). Tumors were scored as illustrated in panel *A* and in Materials and Methods. n = number of animals per group. *D*: Quantification of tumor vascularization in tumors transplanted for 14 days in *Mmp-19*+/+ (black) or *Mmp-19*-/- (white) mice. "d" = distance separating tumor cell layer from the front of migrating blood vessels as defined in panel *A* (see Materials and Methods) (** $P \leq 0.01$, Mann-Whitney test) (n = 8). k: malignant keratinocytes; c: collagen gel; h: host tissue.

Figure 2. Quantification of tumor vascularization and invasion in tumor transplants based on computer-assisted image analysis. *A*: Image processing of a typical transplant section. Malignant keratinocytes (in green) and vessels (in red) (original image) were immunostained according to the procedure described in Materials and Methods. Images are binarized with extraction of vessels (Vascularization) or of tumor cells (Invasion). Tumor vascularization and tumor invasion were determined by using a grid obtained by successive dilatation of the tumor upper border. *B-D*: determination of vessel density ("normalized density of endothelial cells") (*B*) and tumor cell density ("normalized density of tumor cells") (*C, D*) as a function of the distance to the upper boundary of

tumor layer. The maximal distance of tumor cell invasion corresponds to tumor thickness (*D*). Malignant keratinocytes were transplanted into *Mmp-19*+/+ (WT) and *Mmp-19*-/- (KO) mice for 14 days (D14) or 21 days (D21).

Figure 3. BrdU immunostaining of tumor transplants. Malignant keratinocytes were transplanted for 14 days (D14) (*A*) or 21 days (D21) (*B*) into *Mmp-19*+/+ (black) or *Mmp-19*-/- (white) mice. Before sacrifice, mice were injected with BrdU and immunostaining was performed on tumor sections. The percentage of positive cells was determined by a computer-assisted method described in Material and Methods.

Figure 4. *In situ* hybridization of tumor transplants. Sections of malignant keratinocytes transplanted into *Mmp-19*+/+ (*A, B*) and *Mmp-19*-/- (*C*) mice for 21 days were hybridized with 35S-labeled anti-sense *Mmp-19* riboprobe (*A, C*) or sense *Mmp-19* riboprobe (*B*) used as negative control. Bright fields (left) and dark fields (right) images were both captured. Stromal cells in host tissue (h), but not malignant keratinocytes (k) were positively stained for *Mmp-19* mRNAs (original magnification x100).

Figure 5. Immunostaining of tumors transplanted into wild type mice. Sections are counterstained with bisbenzimide (blue staining). Host stromal cells are positive for Mmp-19 immunostaining (in green) (original magnification x200) (*A*). Double immunostainings reveal that Mmp-19 (in red) is not present in newly formed vessels in collagen matrix, but is associated to vascular structures stained with α-smooth muscle actin (α-SMA) antibody (in green) and localized deeply in host tissue (original magnification x400) (*B*). Mmp-19 (in green) does not co-localize with CD11b-positive inflammatory cells (in red) (original magnification x400) (*C*). Higher magnification is shown in insert (*C*).

Figure 6. Increased vascularization in Matrigel Plug containing bFGF and implanted in *Mmp-19-/-* mice. Functional vascularization was quantified by measuring haemoglobin concentration in Matrigel plug implanted into *Mmp-19+/+* and *Mmp-19-/-* mice. * $P \leq 0.05$.

Figure 1

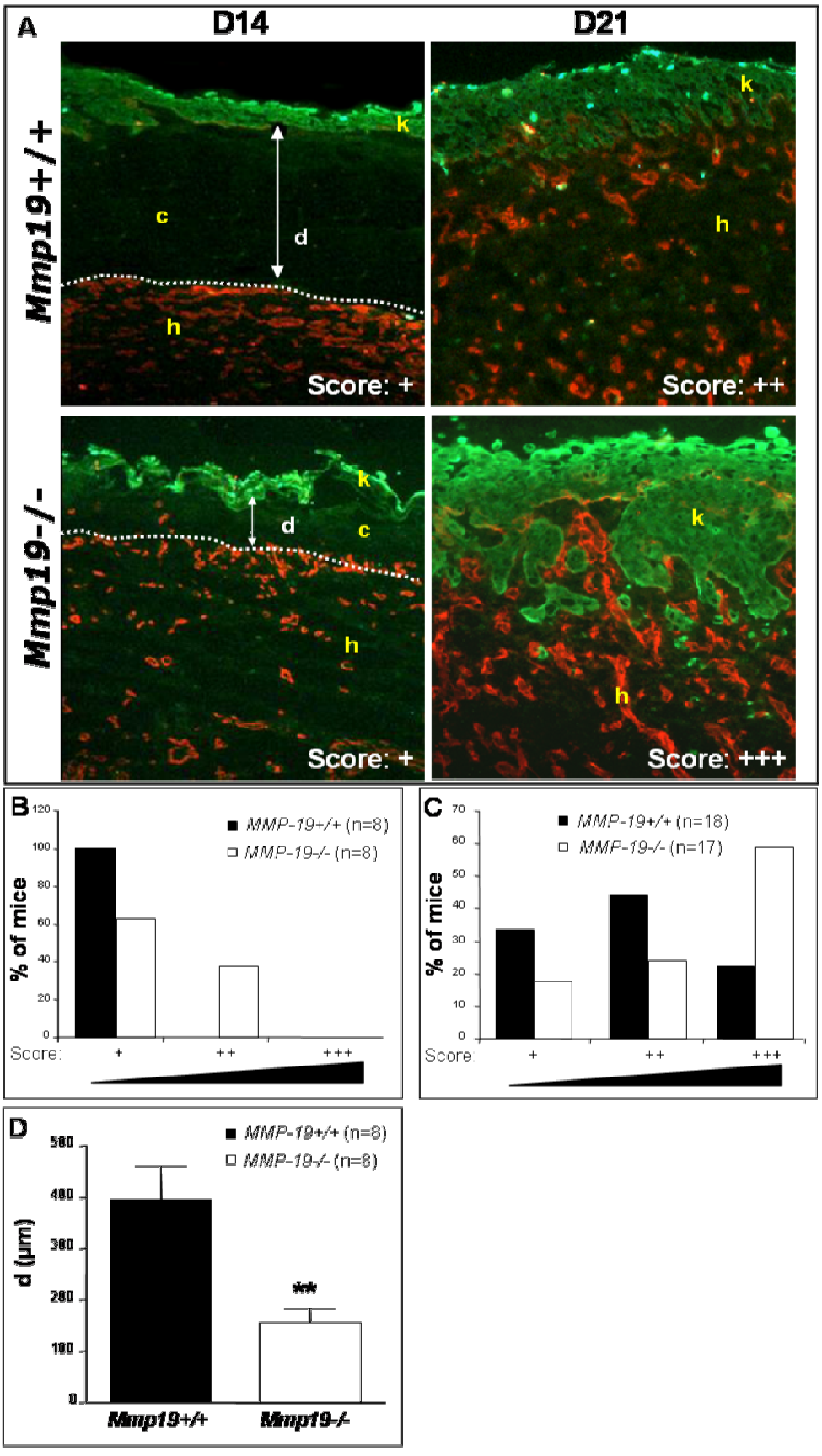
A
D14
D21
Mmp19+/+
Mmp19-/-
k
c
d
h
Score: +
Score: ++
Score: +
Score: +++
B
% of mice
MMP-19+/+ (n=8)
MMP-19-/- (n=8)
Score:
+
++
+++
C
% of mice
MMP-19+/+ (n=18)
MMP-19-/- (n=17)
Score:
+
++
+++
D
d (µm)
MMP-19+/+ (n=8)
MMP-19-/- (n=8)
***
Mmp19+/+
Mmp19-/-

Figure 2

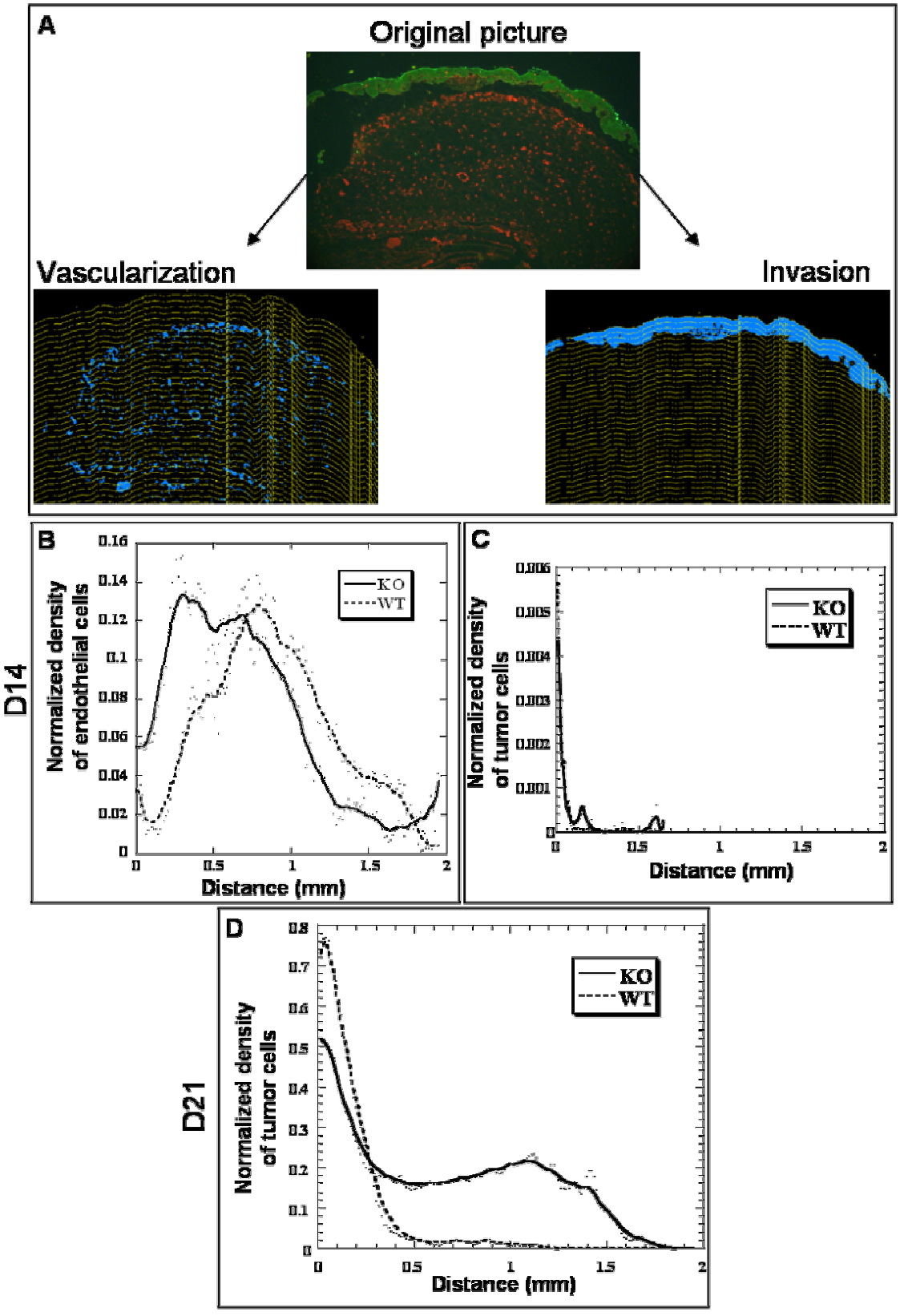
A
Original picture
Vascularization
Invasion
D14
B
Normalized density of endothelial cells
KO
WT
Distance (mm)
C
Normalized density of tumor cells
KO
WT
Distance (mm)
D21
D
Normalized density of tumor cells
KO
WT
Distance (mm)

Figure 3

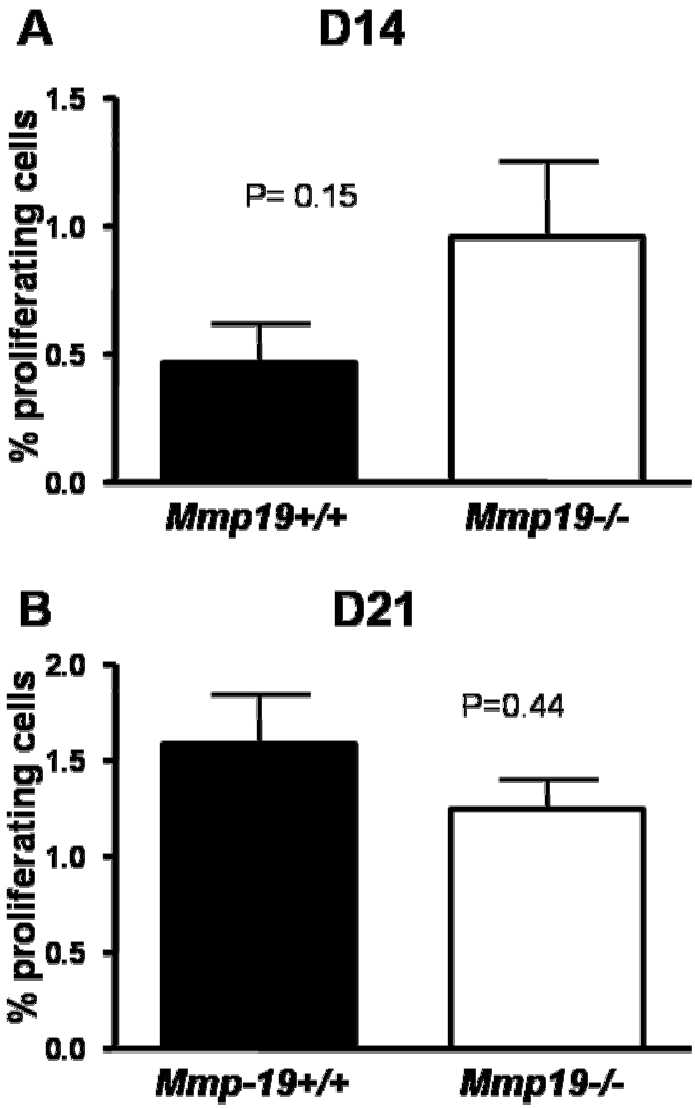
A
D14
% proliferating cells
1.5
1.0
0.5
0.0
P= 0.15
Mmp19+/+
Mmp19-/-
B
D21
% proliferating cells
2.0
1.5
1.0
0.5
0.0
P=0.44
Mmp-19+/+
Mmp19-/-

Figure 4

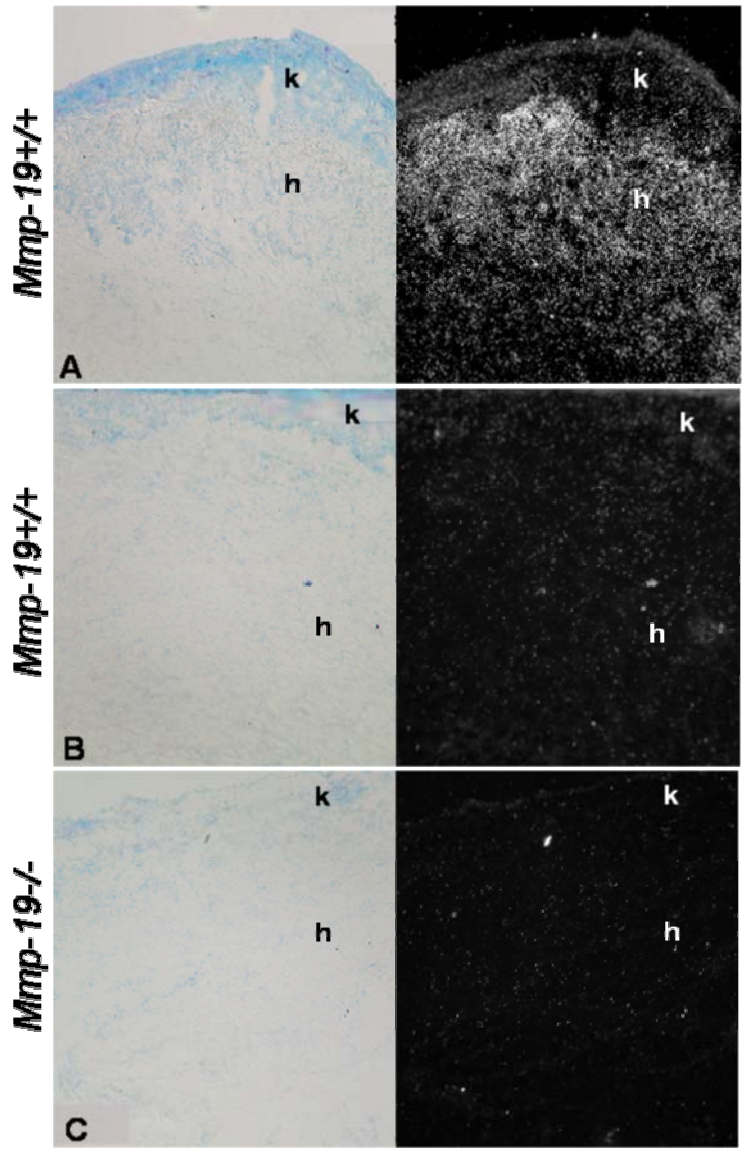

Figure 5

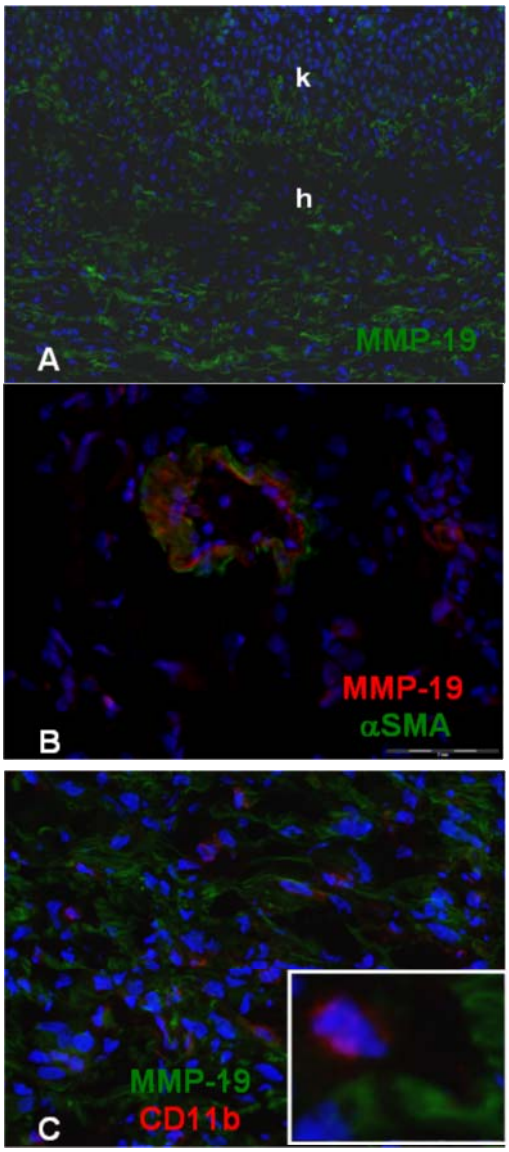

Figure 6

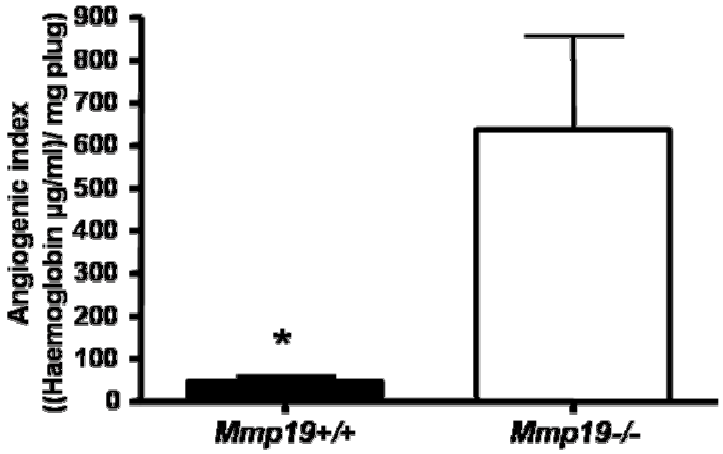
Angiogenic index
((Haemoglobin µg/ml)/ mg plug)
900
800
700
600
500
400
300
200
100
0
*
Mmp19+/+
Mmp19-/-